Industrial Chemistry & Materials

ROYAL SOCIETY OF CHEMISTRY

PAPER

View Article Online
View Journal | View Issue

Cite this: *Ind. Chem. Mater.*, 2025, **3**, 596

Molecular topology-driven benzocyclobutene-based ultralow dielectrics with copper-matched low thermal expansion†

Menglu Li,[ac] Linfeng Fan,[de] Quan Sun,[ac] Meng Xie,[ac] Jin Guo[bc] and Wenxin Fu *[ac]

To address the critical challenge of balancing ultralow dielectric constant (k) with low coefficient of thermal expansion (CTE) in high-frequency electronic applications, this study develops a series of tri-armed benzocyclobutene (BCB)-based resins *via* rational molecular design. Five functional monomers (Ph-BCB, Ph-ene-BCB, Ph-yne-BCB, TPA-yne-BCB, TPB-yne-BCB) were synthesized through Suzuki, Heck, and Sonogashira coupling reactions, followed by thermal curing to form crosslinked polymers. The introduction of branched architectures and rigid conjugated cores effectively enhanced free volume fraction while suppressing molecular chain mobility, achieving synergistic optimization of dielectric and thermomechanical properties. The cured resins exhibited exceptional performance: dielectric constants as low as 1.83 (TPA-yne-BCB) at 1 kHz, dielectric loss below 0.0015, and CTE values ranging from 19.23–34.63 ppm °C^{-1}, closely matching copper (16 ppm °C^{-1}). The SAXS and WAXS analyses confirmed that enlarged free volume and reduced polarization from optimized topology were key to low-k performance. Additionally, the materials demonstrated outstanding thermal stability (5% weight loss >500 °C), high mechanical strength (elastic modulus up to 10 GPa), and hydrophobicity (water absorption <2%). This work provides a groundbreaking strategy for designing high-performance dielectric materials for 5G millimeter-wave packaging, flexible electronics, and 3D heterogeneous integration.

Keywords: Benzocyclobutene; Ultralow dielectric constant; Low thermal expansion; Tri-armed monomer; Branched polymers.

Received 8th April 2025,
Accepted 30th May 2025

DOI: 10.1039/d5im00051c

rsc.li/icm

1 Introduction

To address signal transmission delay and electromagnetic interference in high-density integrated circuits, the International Roadmap for Devices and System specifies that interconnect dielectric materials must achieve a dielectric constant below 2.0 by 2028 and reduce dielectric loss to under 0.002 by 2030.[1] Benzocyclobutene (BCB) resin demonstrates significant application potential in 5G millimeter-wave packaging and flexible electronics due to its exceptional comprehensive properties, including outstanding thermal stability (T_g > 400 °C), water resistance (<0.2% absorption), and dielectric properties (k = 2.65, tan δ = 0.0008).[2–5] However, achieving ultralow dielectric properties while maintaining high-temperature dimensional stability remains a critical bottleneck that hinders its large-scale applications in high-frequency communication modules, 3D heterogeneous integration, and flexible wearable devices.

Two primary approaches exist for reducing dielectric constants: decreasing molecular polarizability[6] and reducing the density of polarizable molecules per unit volume.[7,8] However, these strategies typically increase free volume, subsequently lowering the activation energy for molecular chain segment motion.[9] This fundamentally conflicts with the requirements for low coefficient of thermal expansion (CTE), which demands ordered molecular chain arrangement and dense packing.[10] Specifically, reducing CTE necessitates enhanced intermolecular interactions and improved chain orientation,[11,12] processes that inevitably increase spatial density of polar units and consequently elevate dielectric constant. This inherent contradiction highlights the critical challenge in balancing low dielectric constant with low CTE. Research indicates that introducing rigid aromatic structures at molecular scale can simultaneously achieve low polarizability and high chain orientation,[13] while optimized

[a] *Key Laboratory of Science and Technology on High-Tech Polymer Materials, Institute of Chemistry, Chinese Academy of Sciences, Beijing 100190, China. E-mail: fuwenxin@iccas.ac.cn*
[b] *State Key Laboratory of Polymer Physics and Chemistry, Institute of Chemistry, Chinese Academy of Sciences, Beijing 100190, China*
[c] *University of Chinese Academy of Sciences, Beijing 100049, China*
[d] *Beijing Institute of Space Long March Vehicle, Beijing 100076, China*
[e] *China Academy of Launch Vehicle Technology, Beijing 100076, China*
† Electronic supplementary information (ESI) available. See DOI: https://doi.org/10.1039/d5im00051c

topological design of side chains (*e.g.*, branched or star-shaped architectures) improves the regularity of chain packing while maintaining appropriate free volume.[14,15]

Branched polymers demonstrate remarkable structure–property advantages in functional materials for biomedical applications,[16,17] lithium batteries,[18] coatings,[19] films,[20] and composite processing[21] due to their unique three-dimensional topological architectures. Their branched structures create abundant intramolecular cavities that effectively reduce chain entanglement and promote free volume formation, thereby enhancing dielectric performance.[22–24] Lee *et al.*[23] introduced aliphatic diamines into the synthesis of copolyimides. The branched large aliphatic unit expands the free volume, effectively reduces the dipole moment density, and successfully reduces the dielectric constant from 2.7 to 2.49. At the same time, the non-covalent interaction between the aliphatic chain effectively inhibits the chain movement and reduces the dielectric loss. Furthermore, precise polymer backbone design enables fine-tuned material properties.[25] Rigid backbone structures significantly suppress chain folding and entanglement. For example, He *et al.*[26] showed that the tight packing of rigid polymer skeleton limits the deflection of dipoles in the electric field, which can effectively reduce dielectric loss. Zhou *et al.*[10] demonstrated that the 3D continuous branched skeleton formed by the rigid cross-linked structure can limit the movement of the chain, thereby reducing CTE. However, the permittivity of polyimide with micro branched structure is still greater than 3 and the dielectric loss is greater than 0.005. That is to say, although the branched polymers naturally have many advantages, they still cannot combine the comprehensive characteristics of low dielectric constant, low dielectric loss, low CTE, high heat resistance and high mechanical properties at the same time. These limitations underscore the need for molecular designs that integrate topological freedom with structural rigidity.

Herein, we propose a tri-armed BCB resin platform combining branched topology structure and conjugated cores to synergistically optimize dielectric and thermomechanical properties. By functionalizing rigid aromatic cores (*e.g.*, triphenylamine) with triple-bond-bridged BCB arms, we aimed to (1) amplify free volume *via* controlled branching, (2) suppress polarization through restricted chain dynamics, and (3) enhance crosslinking density for dimensional stability. Five monomers (Ph-BCB, Ph-ene-BCB, Ph-yne-BCB, TPA-yne-BCB, TPB-yne-BCB) were synthesized to systematically investigate the effects of bridging bonds (single/double/triple) and core size on performance. The synergistic effect between cured BCB groups and inherent rigid backbones of these monomers effectively prevent molecular packing distortion and polarization while promoting free volume fraction enhancement – a critical for achieving low dielectric performance. Concurrently, it significantly restricted molecular chain mobility, resulting in substantially reduced CTE. The optimized TPA-yne-BCB resin achieved a breakthrough dielectric constant of 1.83 (at 1 kHz) with low CTE, outperforming state-of-the-art BCB derivatives and commercial polymers. This work not only resolves the long-standing *k*-CTE trade-off but also provides a scalable molecular design strategy for high-frequency electronic packaging.

2 Results and discussion

2.1 Synthesis and characterization of monomers and their cross-linking and curing behavior

Scheme 1 shows a schematic diagram of the chemical structures and synthetic routes of tri-armed BCB-based

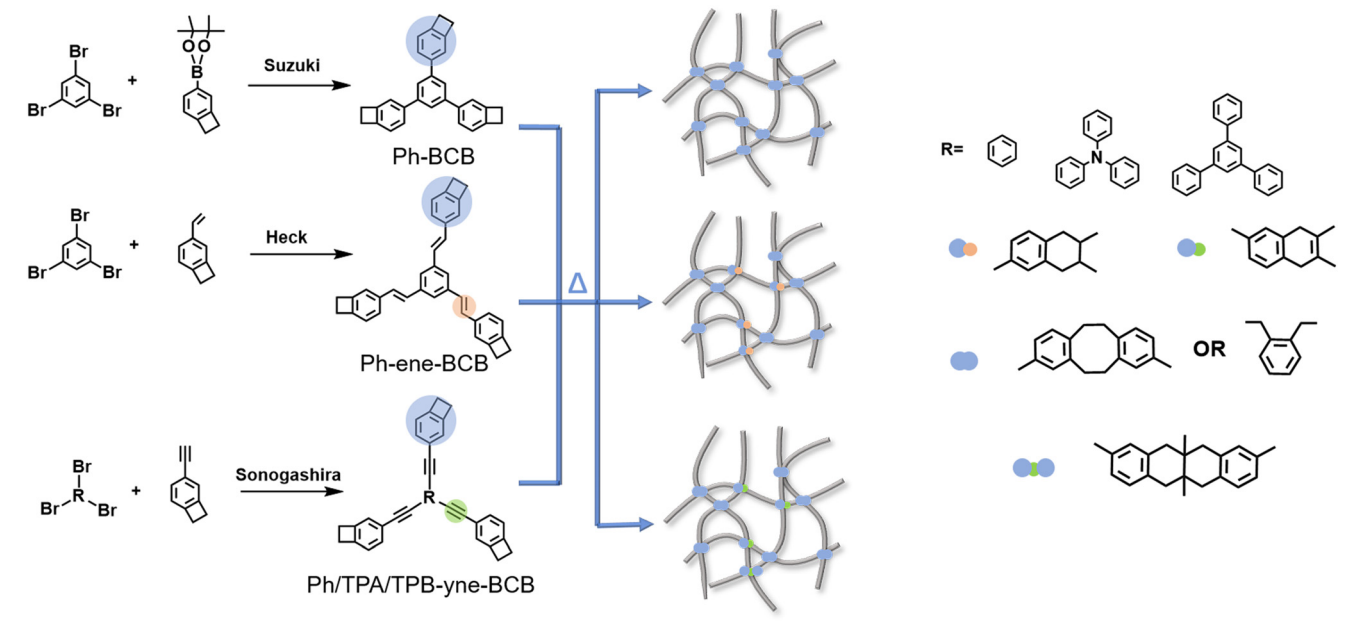

Scheme 1 Synthesis and polymerization of tri-armed BCB-based monomers.

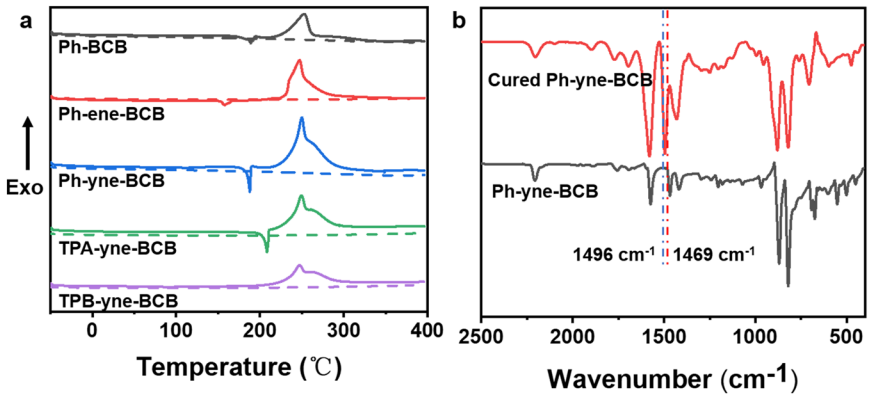

Fig. 1 (a) DSC curves of monomers (solid line: the first heating process; dashed line: second heating process); (b) FTIR spectra of Ph-yne-BCB and cured Ph-yne-BCB.

target monomers. The target monomers Ph-BCB, Ph-ene-BCB, Ph-yne-BCB, TPA-yne-BCB, TPB-yne-BCB were synthesized by the palladium catalyzed Suzuki, Heck and Sonogashira reaction, and then purified by column chromatography to give rise to Ph-BCB, Ph-ene-BCB, Ph-yne-BCB, TPA-yne-BCB, TPB-yne-BCB with yields of 82%, 47%, 77%, 75%, 72%. ^{1}H NMR, ^{13}C NMR and MALDI-TOF were used to characterize and validate the chemical structures of all final products, as shown in Fig. S3–S7.†

DSC was used to monitor the curing process of all monomers, and the results were shown in Fig. 1a. It can be seen from the results that during the first temperature rise of the three monomers with different bonding structures, there's an endothermic peak and an exothermic peak. The melting peak temperatures of Ph-BCB, Ph-ene-BCB and Ph-yne-BCB are 188.97 °C, 157.45 °C and 187.76 °C, respectively. The difference is that Ph-yne-BCB exhibits a shoulder during the exothermic process, which is related to the polymerization of three bonds in the structure.[27] In addition, among the three monomers with different cores, Ph-yne-BCB and TPA-yne-BCB both contain melting phase transformation process, and the melting peak temperature is 188.76 °C and 208.28 °C, respectively. With the increase of the number of benzene rings, the peak temperature increases. Since TPB-yne-BCB has the most benzene rings in its molecular structure, there is no melting process before solidification. As the temperature continued to rise, exothermic peaks appeared in all three monomers, which was consistent with the ring-opening temperature of BCB group.[28] At the same time, a shoulder peak appears at about 264 °C, which further proves that the heat release at this time is related to the polymerization of three bonds in the molecule. Finally, no obvious exothermic peak is found in the second scan of all monomers, indicating that they are completely cured.[29]

The complete cross-linking reaction was further confirmed by FTIR spectroscopy (Fig. 1b). Taking Ph-yne-BCB monomer as an example, the characteristic absorption peak of the four-member ring disappears at 1469 cm^{-1}. At the same time, a new absorption peak appears at 1496 cm^{-1}, which is caused by the C–H deformation vibration of the six-membered ring. It shows that the four-membered ring reacts with the double bond to form a six-membered ring. The above analysis shows that there is no quaternary ring left after thermal curing.

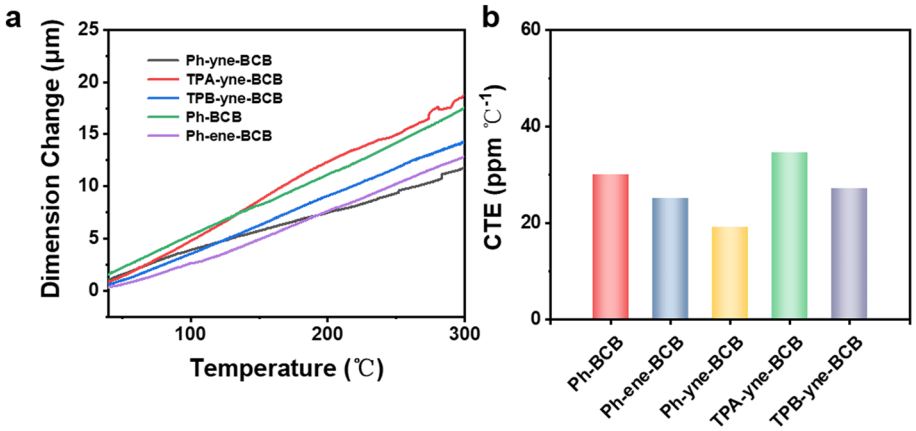

Fig. 2 TMA curves (a) and coefficient of thermal expansion (b) of cured resins.

2.2 Thermal mechanical properties

As an insulating dielectric material between layers, dimensional stability is very important. TMA was used to test the CTE of the materials under nitrogen atmosphere to characterize the dimensional stability in the range of 40–300 °C. Fig. 2 shows the curve of all material shape variables with temperature. It can be seen that the deformation of all materials increases linearly with the increase of temperature, and the slope of the curve remains unchanged within the test temperature range, indicating that the T_g of all materials are greater than 300 °C and all materials have excellent thermal properties.

It can be seen from the test results that all resins have excellent dimensional stability, CTE is less than 34.63 ppm $°C^{-1}$, and the minimum value can reach 19.23 ppm $°C^{-1}$, which is very close to the CTE of copper (16 ppm $°C^{-1}$). This is beneficial to the application in the field of interlayer insulation materials, and also meets the original intention of molecular design in this paper. Compared with BCB resins containing different indirect structures, the CTE of Ph-BCB, Ph-ene-BCB and Ph-yne-BCB were 30.01, 25.05 and 19.23 ppm $°C^{-1}$, respectively, because the cross-linking degree of the material increased. This dense structure is helpful to maintain that the material size does not change significantly with increasing temperature, so the CTE gradually decreases. Then, compared with BCB resins with three bonds as a bridge structure and containing different conjugated cores, the CTE of Ph-yne-BCB, TPA-yne-BCB and TPB-yne-BCB were 19.23, 34.63 and 27.09 ppm $°C^{-1}$, respectively. Due to the enlargement of conjugated cores, larger pores are generated, which leads to the increase of CTE in both TPA-yne-BCB and TPB-yne-BCB to a certain extent. By contrast, TPA-yne-BCB has a larger free volume, so its CTE is the largest, but it also meets the application requirements of interlayer insulating dielectric materials.

2.3 Dielectric properties

After the purified monomers were prepolymerized, the circular sheets with uniform thickness was prepared by thermal cross-linking curing. The dielectric properties of the materials were measured by parallel plate capacitor method. Fig. 3a and Fig. 3d show the change curve of the dielectric constant and dielectric loss of all samples in the frequency range of 1 Hz–1 MHz, as well as the dielectric constant and dielectric loss of the material at 1 kHz (Fig. 3b and e). It can be clearly seen that all materials have low dielectric constant (<2.5) and dielectric loss (<0.0015), and the dielectric constant does not change with frequency. This is better than the dielectric properties of most dense polymers, such as polyimide,[30] epoxy resin,[31] BCB resin,[32] *etc.* However, due to subtle differences in the chemistry and molecular structure of the molecules, their dielectric properties are also different at a given frequency.

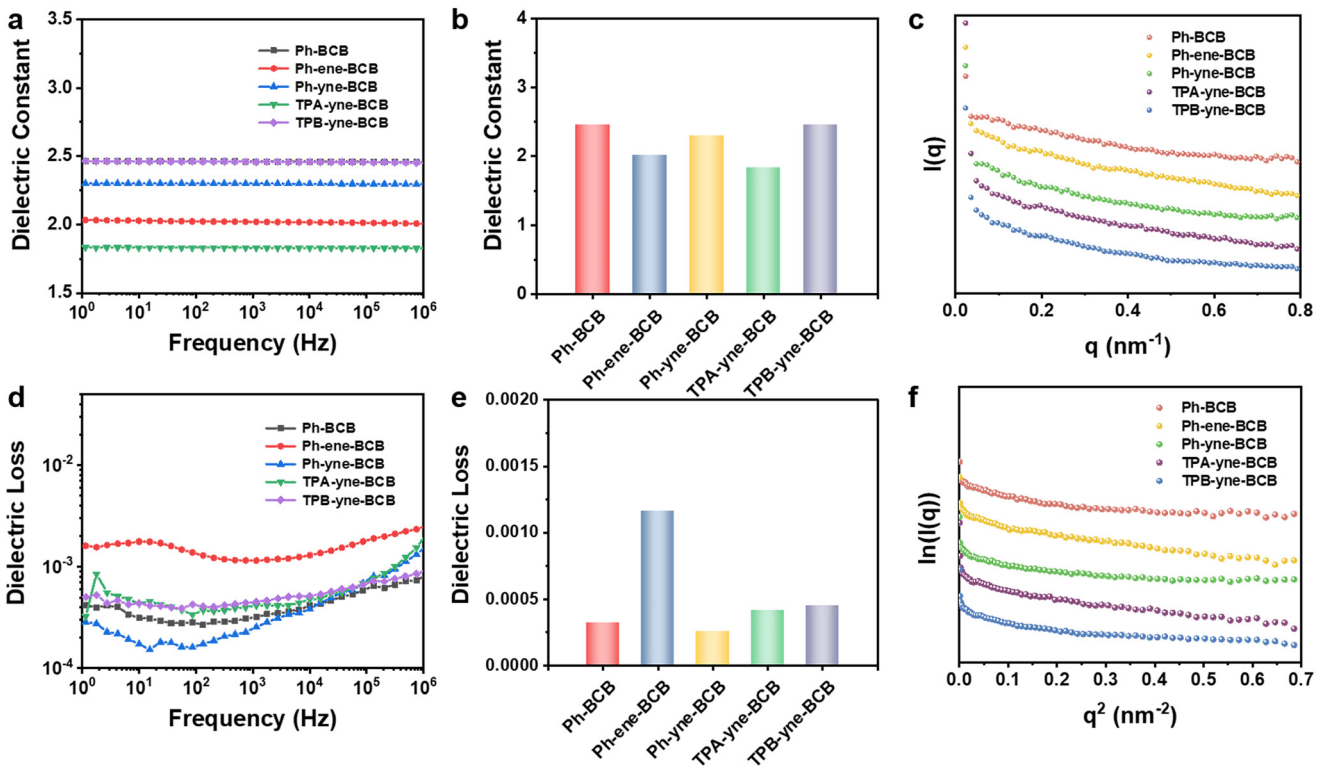

Fig. 3 Dielectric constant (a) and dielectric loss (d) of the cured resins with frequency; dielectric constant (b) and dielectric loss (e) of the cured resins at 1 kHz; SAXS pattern (c) and the variation of ln($I(q)$) with q^2 (f) of the cured resins.

We compare the dielectric constant of all materials at 1 kHz, as shown in Fig. 3b. Among the three molecules with different bonding structures, Ph-ene-BCB has the lowest dielectric constant, followed by Ph-yne-BCB, and Ph-BCB has the highest dielectric constant, with the dielectric constant of 2.02, 2.30 and 2.46 respectively. This is because compared with Ph-BCB, Ph-ene-BCB and Ph-yne-BCB have longer molecular arms due to the addition of double or triple bond bonding structures, so they can form a larger free volume after cross-linking curing, so the dielectric constant is lower. This was further demonstrated by the characterization of the microstructure of the fully cured material by WAXS, as shown in Fig. S8.† The *d*-spacing reflects the average distance between polymer segments and is related to the free volume. The diffraction peak of Ph-ene-BCB is concentrated at the minimum q = 0.48 nm^{-1}, and according to the Bragg equation,[33] the corresponding average chain spacing is the largest, which is 13.09 nm, indicating that the bond structure of the double bond can produce a larger molecular chain spacing with a larger free volume. In addition, the presence of unsaturated dienophile bodies (double or triple bonds) can cross-link with BCB groups to increase the cross-linking density of the material, thus limiting the molecular chain motion and reducing the polarization of the dipole, which is also conducive to the reduction of the dielectric constant.[34] On the other hand, compared with Ph-ene-BCB, a triple bond in Ph-yne-BCB molecule can provide two reaction sites for the BCB group, and multiple reaction possibilities reduce the free volume of the material, so the dielectric constant of Ph-yne-BCB is relatively larger. However, among the three materials, although the dielectric constant of Ph-ene-BCB is the smallest, its dielectric loss is the largest, which is 1.16 × 10^{-3}. Therefore, the dielectric constant and dielectric loss are investigated in a comprehensive way, and three bonds are selected as the bonding structure connecting the molecular core and BCB group, so as to further explore the influence of the molecular core on dielectric properties.

Among the three molecules with different conjugated cores, TPA-yne-BCB has the lowest dielectric constant, followed by Ph-yne-BCB, and TPB-yne-BCB has the highest dielectric constant, with the dielectric constant of 1.83, 2.30 and 2.46 respectively. By adjusting the core size, the dielectric constant is further reduced to below 2.0, achieving a breakthrough in ultra-low dielectric constant materials, which is very rare in non-porous low dielectric materials at present. This is because, on the basis of Ph-yne-BCB, we chose triphenylamine with a larger structure as the core, which can form a larger molecular skeleton after curing, thus generating more free volume and further reducing the dielectric constant. WAXS results of the material also calculated the largest intermolecular chain spacing. Compared with TPB-yne-BCB, although the triphenylbenzene has a larger volume, the rotation of the three single bonds connected by nitrogen atoms in the triphenylamine structure is more flexible, which can cause obvious steric hindrance, so that the reaction degree of the three bonds in the curing process is lower, and the free volume is larger.[35] At the same time, large steric hindrance can also limit the migration of molecular chain segments and reduce the orientation of dipoles, thus reducing the overall polarization of the material, so the dielectric constant is lower.

In order to further prove the relationship between the free volume and dielectric constant of the material, we used SAXS to analyze the molecular microstructure inside the material. Fig. 3c shows the curve of the small-angle scattering intensity $I(q)$ of the material as a function of q value. As q increases, $I(q)$ gradually decrease, showing typical small-angle X-ray scattering behavior. This indicates that there are indeed scatterers with uneven electron density at the nanoscale in the five material systems due to differences in internal microstructure. Since the system is a homogeneous system, this uneven electron density comes from differences in molecular structure. According to Guinier's law,[36] in a monodisperse scattering system, the scattering intensity in the small q region can be expressed by the following formula:

$$I(q) = I(0)\exp\left(-\frac{1}{3}R_g^2 q^2\right) \quad (1)$$

where $I(0)$ is the scattering intensity when q is 0, and R_g is the rotation radius of the scatterer, which is used to measure the characteristic size of the scatterer. Taking the logarithm of both sides of the equation at the same time gives the following formula:

$$\ln I(q) = \ln I(0) - \frac{1}{3}R_g^2 q^2 \quad (2)$$

It can be seen from eqn (2) that when the system follows Guinier's law, $\ln I(q)$ has a linear relationship with q^2, and the radius of rotation of the material can be obtained by fitting the slope of $\ln I(q) - q^2$.

The $\ln I(q) - q^2$ curve is shown in Fig. 3f. It shows a good linear relationship in a large q region, indicating that the five

Table 1 Dielectric properties, SAXS parameters and density of resins

	k	tan (δ)	$k_{\ln(I(q))-q^2}$	R_g (nm)	ρ (g cm^{-2})
Ph-BCB	2.46	3.21×10^{-4}	−1.103	1.82	1.165
Ph-ene-BCB	2.02	1.16×10^{-3}	−1.379	2.03	1.077
Ph-yne-BCB	2.30	2.56×10^{-4}	−0.959	1.70	1.121
TPA-yne-BCB	1.83	4.16×10^{-4}	−1.423	2.07	1.006
TPB-yne-BCB	2.46	4.53×10^{-4}	−0.946	1.68	1.168

material systems are all uniform monodisperse systems. The curve slopes and gyration radii calculated are listed in Table 1. From the calculation results, it can be seen that the gyration radii of Ph-BCB, Ph-ene-BCB and Ph-yne-BCB are 1.82, 2.03 and 1.70 nm, respectively. The larger the gyration radius, the greater the rigidity of the molecular chain and the larger the free volume in the cured material.[37] Therefore, the dielectric constant of Ph-ene-BCB is the smallest among the three. Similarly, the gyration radii of Ph-yne-BCB, TPA-yne-BCB and TPB-yne-BCB are 1.70, 2.07 and 1.68 nm, respectively, which are in good consistency with the relative size of the dielectric constants among the three. Meanwhile, macroscopically, the dielectric constants of the five materials decrease as the density increases. The elaboration of dielectric constant and density in the Clausius-Mossotti equation[38] can well explain this phenomenon.

2.4 Hydrophobicity, thermostability and mechanical property

The working environment of electronic components makes the hydrophobicity of materials a very important performance indicator, and strong hydrophobicity is a necessary condition for protecting electronic equipment from moisture. The hydrophobicity of the five cured resins was evaluated by the static contact angle and water absorption of the materials, as shown in Fig. 4a and d. The results showed that all the resins had good hydrophobic properties, and the water absorption rate was <2% and the static contact angle was >108° after soaking at room temperature for 24 h.

TGA was used to determine the thermal stability of the resin material in a nitrogen atmosphere (Fig. 4b and e and S9†). It can be seen from the test results that the thermal stability of all resins is very good, the temperature of thermal weight loss of 5% is greater than 500 °C, and the carbon residue rate is greater than 67.7% at 800 °C. It is worth noting that changing the bonding structure of the molecule is more effective in improving thermal stability. The thermal decomposition temperatures of Ph-yne-BCB, TPA-yne-BCB and TPB-yne-BCB are as high as 641.6 °C, 590.8 °C and 617.2 °C when the triple bonds are used as the bridge structure. At 800 °C, the carbon residue rates were 92.2%, 89.6% and 91.1%, respectively. This is because the existence of triple bonds improves the cross-linking density of the system, and many structures such as biphenyls and naphthalene rings are formed after cross-linking and curing in the molecule, which greatly improves the thermal stability of the cross-linked resin.

Finally, the mechanical properties of the materials were evaluated by nanoindentation technology (Fig. 4c and f and S10†). From the test results, it can be seen that all resins have excellent mechanical properties, thanks to the high cross-linking density and aromatic structure of the resins.

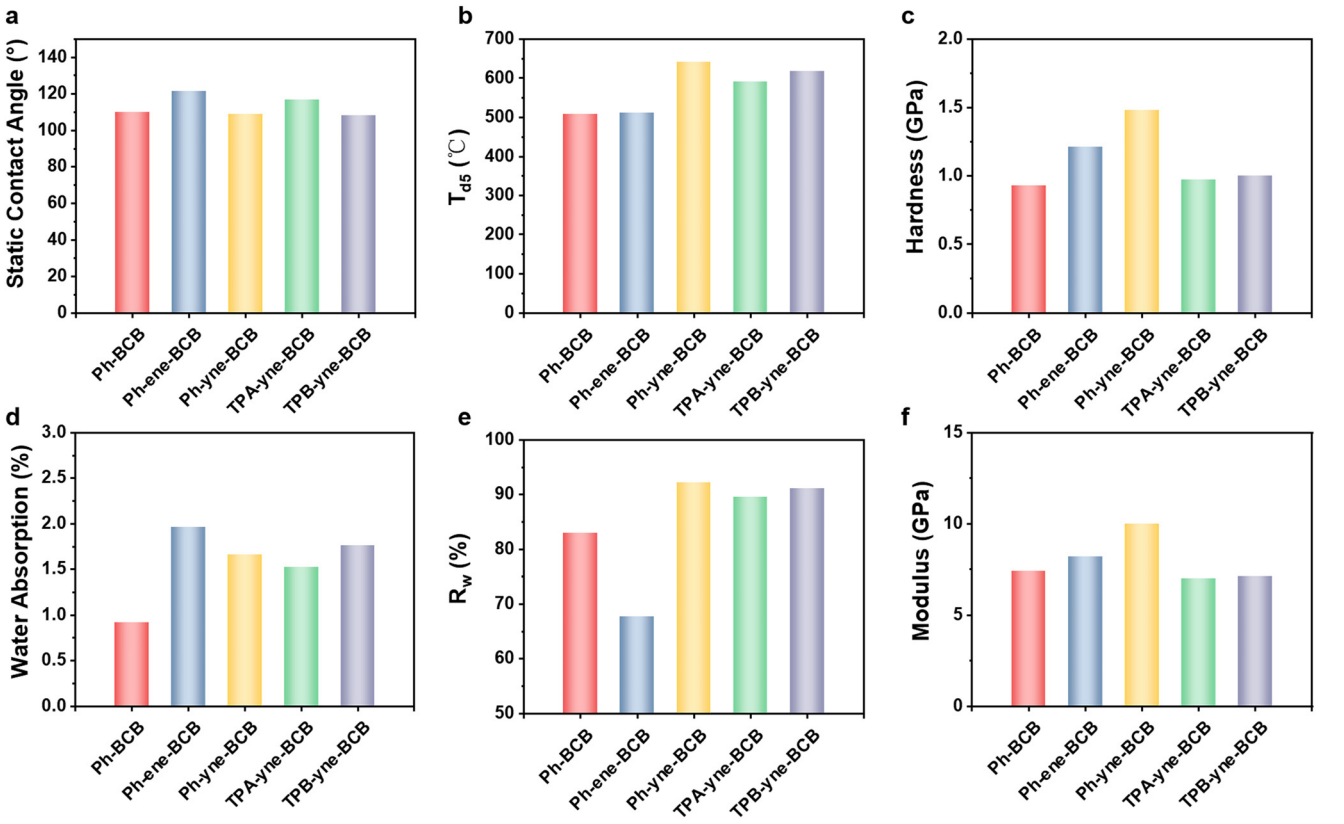

Fig. 4 Hydrophobicity (static contact angle (a), water absorption (d)), thermostability (5% weight loss (b), char yield at 800 °C (e)) and mechanical property (hardness (c), modulus (f)) of cured resins.

Compared with BCB resins with different bonding structures, the hardness of Ph-BCB, Ph-ene-BCB and Ph-yne-BCB were 0.93 GPa, 1.21 GPa and 1.48 GPa, and the elastic modulus were 7.4 GPa, 8.2 GPa and 10 GPa, respectively. The change trend of both materials is the same with the material structure. It can be seen that the system with triple bonds as the bridge structure has higher crosslinking density and better mechanical properties. Therefore, on the basis of triple bond structure, we explore the influence of different conjugated cores on the mechanical properties of materials. According to the test results, the hardness of Ph-yne-BCB, TPA-yne-BCB and TPB-yne-BCB are 1.48 GPa, 0.97 GPa and 1 GPa respectively, and the elastic modulus are 10 GPa, 7 GPa and 7.1 GPa respectively. This is because, with the increase of the volume of the conjugated core, the molecular cross-linking curing can form larger pores, which is not conducive to the mechanical properties of the material. At the same time, TPA-yne-BCB has a more flexible molecular structure and can produce a larger free volume, so the mechanical properties are slightly worse than TPB-yne-BCB.

3 Conclusions

In this work, we demonstrated that molecular topology engineering of tri-armed benzocyclobutene (BCB) resins effectively reconciles the long-standing conflict between ultralow dielectric constant and low thermal expansion coefficient. By integrating rigid conjugated cores (*e.g.*, triphenylamine) with triple-bond-bridged BCB arms, the optimized TPA-yne-BCB resin achieved a record-low k of 1.83 at 1 kHz (dielectric loss < 0.0005) and the Ph-yne-BCB resin achieved a copper-matched CTE = 19.23 ppm $°C^{-1}$, surpassing conventional polymers like polyimide and epoxy ($k > 2.5$, CTE $>$ 50 ppm $°C^{-1}$). SAXS/WAXS analysis and Guinier modeling reveal that the enlarged free volume (R_g = 2.07 nm) and restricted chain mobility synergistically minimize polarization while maintaining dimensional stability. Moreover, the materials exhibit exceptional thermal resilience (5% weight loss >500 °C), mechanical robustness (elastic modulus up to 10 GPa), and hydrophobicity (water absorption <2%), fulfilling stringent requirements for harsh operational environments.

This study establishes a molecular design paradigm where branched architectures and rigid conjugated units cooperatively modulate both dielectric and thermomechanical properties. The scalable synthesis route and simple thermal curing further enhance industrial viability. Future work will focus on integrating these resins into multilayer circuit prototypes to validate signal integrity at millimeter-wave frequencies, as well as exploring dynamic covalent chemistry to enable recyclability. By bridging the gap between molecular-scale design and macroscopic performance, this strategy opens new avenues for advanced dielectric materials in 5G/6G communication modules, flexible hybrid electronics, and sustainable packaging technologies.

4 Experimental section

4.1 Materials

Copper(I)iodide (CuI, 99.5%), potassium acetate (KOAc, 99%), dimethyl sulfoxide (anhydrous DMSO, 99.9%, water ≤ 50 ppm), tetrahydrofuran (anhydrous THF, 99.9%, water ≤ 50 ppm), *N*,*N*′-dimethylformamide (anhydrous DMF, 99.9%, water ≤ 50 ppm) were provided by Beijing InnoChem Science & Technology Co., Ltd. Palladium(II)acetate ($Pd(OAc)_2$, 98%) were purchased from Sigma-Aldrich. Bis(pinacolato)diboron (98%), 1,3,5-tribromobenzene (98%), 1,3,5-tris (4-bromophenyl)benzene (98%), tris(4-bromophenyl)amine (98%), di-chlorobis(triphenylphosphine)palladium(II) ($Pd(PPh_3)_2Cl_2$, 98%), 1,1′-[Bis (diphenylphosphino)ferrocene] dichloropalladium(II) ($Pd(dppf)_2Cl_2$, 98%), tri(*o*-tolyl) phosphine ($P(o\text{-tolyl})_3$, 98%) was obtained from Energy Chemical. Potassium carbonate (K_2CO_3, >99.0%), sodium chloride (NaCl, 99.5%), magnesium sulfate ($MgSO_4$, ≥98.0%) was provided by Sinopharm Chemical Reagent Co., Ltd. Trimethylsilylacetylene (97%) were purchased from J&K Scientific Ltd. Triphenylphosphine (PPh_3, >99.0%) was obtained from Shanghai Macklin Biochemical Technology Co., Ltd. 4-bromobenzocyclobutene (4-BrBCB, 97%) was provided by Beichuan Tianxun New Material Co., Ltd. 4-vinylbenzocyclobutene (4-VBCB, 98%) was provided by Mianyang ChemTarget Technology Co., Ltd. Triethylamine, dioxane, dichloromethane, petroleum ether, ethyl acetate, methyl alcohol, ethyl alcohol were purchased from Concord Technology (Tianjin) Co., Ltd. Triethylamine was dried at room temperature with anhydrous calcium hydride for 12 h and use immediately after distillation.

4.2 Characterization

^1H and ^{13}C nuclear magnetic resonance (NMR) spectra were acquired on a Bruker Fourier 300 MHz NMR spectrometer (Switzerland) using tetramethylsilane (TMS) as the internal reference. Matrix-assisted laser desorption ionization time-of-flight (MALDI-TOF) mass spectra was carried out on a Bruker BIFLEX III system using positive reflection mode or linear mode with a 337 nm nitrogen laser. Fourier transform infrared (FTIR) spectra were recorded on a Bruker Tensor-27 FTIR spectrometer in the range of 4000–400 cm^{-1}. The KBr tablet was as a background. Differential scanning calorimetry (DSC) was performed on a TA Q2000 calorimeter in a nitrogen atmosphere. About 5 mg of sample were heated from 40 to 400 °C using the heating rate of 10 °C min^{-1}. Thermogravimetric analyses measurements (TGA) were carried out on a TA Q600 Instrument using ~5 mg of samples at a heating rate of 10 °C min^{-1} from 40 to 800 °C under N_2 atmosphere. The coefficient of thermal expansion (CTE) was determined on a Setsys Evo TMA at a heating rate of 5 °C min^{-1} from 40 °C to 400 °C in N_2. The nanoindentation test was characterized by Keysight G200 technology, and the

maximum penetration depth was about 2000 nm. The dielectric constant and dielectric loss of the samples (Ø35 mm × 0.3 mm) were tested using a Novocontrol Concept 40 broadband dielectric impedance spectrometer with frequencies ranging from 1 Hz to 1 MHz. SAXS/WAXS was determined by Xenocs Xeuss 2.0. The copper target Cu/Kα was used as the light source in the system, and the wavelength was 1.54189 Å. The density was tested using a density balance (Qunlong, LSD 100E). Before the test, all materials were dried in a vacuum oven at 100 °C for 24 hours to remove moisture. Static contact angle measurements were performed using a KRÜSS DSA 100 instrument (Germany). Water absorption was characterized by weighing the mass of samples before and after immersion in water at room temperature after 24 h.

4.3 Synthesis of 4-ethynyl benzocyclobutene

Add 4-bromobenzocyclobutene (18.3 g, 0.1 mol) to a pre-dried three-neck flask, then add 150 mL of triethylamine to the flask. After bubbling with N_2 for 15 min in an ice-water bath to deoxygenate, add trimethylsilylacetylene (14.733 g, 0.15 mol), $Pd(PPh_3)_2Cl_2$ (1.4 g, 2 mmol), and CuI (0.19 g, 1 mmol), and continue bubbling with N_2 for another 15 min. Under nitrogen protection, the system is slowly heated to 90 °C and left to react for 12 h. After cooling to room temperature, filter out the insoluble solids from the system, add 100 mL of dichloromethane for dissolution, extract three times with saturated sodium chloride solution, and dry the organic phase with anhydrous magnesium sulfate for 2 h. Filter and rotary evaporate to remove the solvent. Dissolve the obtained crude product in 500 mL of methanol, add anhydrous potassium carbonate (13.882 g, 0.1 mol), and stir at room temperature for 5 h. Filter out the insoluble solids from the system, rotary evaporate to remove excess solvent, then dissolve the resulting solid in 100 mL of dichloromethane, extract three times with saturated sodium chloride solution, and dry the organic phase with anhydrous magnesium sulfate for 2 h. Filter, rotary evaporate, and column chromatography (eluent: petroleum ether = 1 : 50) to obtain a light yellow liquid with a yield of 90%. ^{1}H NMR ($CDCl_3$, 300 MHz, δ, ppm): 3.02 (s, 1H), 3.18 (s, 4H), 6.99–7.02 (d, 1H), 7.18 (s, 1H), 7.34–7.36 (d, 1H).

4.4 Synthesis of 4-borate benzocyclobutene

Add 4-bromobenzocyclobutene (18.3 g, 0.1 mol), bis(pinacolato)diboron (28 g, 0.11 mol), and potassium acetate (29.4 g, 0.3 mol) to a pre-dried three-neck flask, then add 100 mL of anhydrous DMSO. After bubbling with N_2 for 15 min in an ice-water bath to deoxygenate, add $Pd(dppf)_2Cl_2$ (1.09 g, 1.5 mmol), and continue bubbling with N_2 for another 15 min. Under nitrogen protection, slowly raise the temperature of the system to 80 °C and let it react for 6 h. After cooling to room temperature, filter out the insoluble solids from the system, add 100 mL of ethyl acetate, extract three times with saturated sodium chloride solution, dry the organic phase by rotary evaporation, then add 100 mL of dichloromethane for dissolution, continue extracting three times with saturated sodium chloride solution, and finally dry the organic phase with anhydrous magnesium sulfate for 2 h. Filter, rotary evaporate, and perform column chromatography (eluent: ethyl acetate/petroleum ether, ratio 1 : 50) to obtain a pale yellow liquid with a yield of 74%.^{1}H NMR ($CDCl_3$, 300 MHz, δ, ppm): 1.36 (s,12H), 3.20 (s, 4H), 7.07–7.09 (d, 1H), 7.52 (s, 1H), 7.70–7.72 (d, 1H).

4.5 Synthesis of Ph-BCB

Place 1,3,5-tribromobenzene (3.15 g, 10 mmol), 4-borate benzocyclobutene (13.8 g, 60 mmol), and sodium carbonate (8 g, 75 mmol) into a pre-dried three-neck flask, then add 20 mL of water, 40 mL of ethanol, and 80 mL of dioxane to the flask. After bubbling with N_2 for 15 min in an ice-water bath to deoxygenate, add $Pd(PPh_3)_4$ (0.87 g, 0.75 mmol), and continue bubbling with N_2 for another 15 min. Under nitrogen protection, slowly raise the temperature of the system to 110 °C and let it react for 24 h. After cooling to room temperature, remove excess solvent by rotary evaporation, then dissolve the remaining solid in 100 mL of dichloromethane, extract three times with saturated sodium chloride solution, and dry the organic phase with anhydrous magnesium sulfate for 2 h. Filter, rotary evaporate, and perform column chromatography (eluent: dichloromethane/petroleum ether, ratio 1 : 20 to 1 : 5) to obtain a white powder with a yield of 82%.^{1}H NMR ($CDCl_3$, 300 MHz, δ, ppm): 3.24 (s, 12H), 7.14–7.16 (d, 3H), 7.37 (s, 3H), 7.50–7.52 (d, 3H), 7.67 (s, 3H); ^{13}C NMR ($CDCl_3$, 75 MHz, δ, ppm): 29.48 (s), 29.54 (s), 121.77 (s), 122.83 (s), 125.10 (s), 126.34 (s), 140.44 (s), 143.28 (s), 145.17 (s), 146.33 (s); MALDI-TOF MS (m/z) Calcd: for $C_{30}H_{24}$, 384.522; found: 384.064.

4.6 Synthesis of Ph-ene-BCB

Place 1,3,5-tribromobenzene (6.3 g, 20 mmol), 4-vinylbenzocyclobutene (8.6 g, 66 mmol), and triethylamine (30 g, 0.3 mol) into a pre-dried three-neck flask, then add 60 mL of DMF to the flask. After bubbling with N_2 for 15 min in an ice-water bath to deoxygenate, add $Pd(OAc)_2$ (0.68 g, 3 mmol) and $P(o\text{-tolyl})_3$ (2.74 g, 9 mmol), and continue bubbling with N_2 for another 15 min. Under nitrogen protection, slowly raise the temperature of the system to 115 °C and let it react for 12 h. After cooling to room temperature, filter out the insoluble solids from the system, remove excess solvent by rotary evaporation, then dissolve the remaining solid in 100 mL of dichloromethane, extract three times with saturated sodium chloride solution, and dry the organic phase with anhydrous magnesium sulfate for 2 h. Filter, rotary evaporate, and perform column chromatography (eluent: dichloromethane/petroleum ether, ratio 1 : 20 to 1 : 5) to obtain a white powder with a yield of 47%. ^{1}H NMR ($CDCl_3$, 300 MHz, δ, ppm): 3.21 (s, 12H),

7.05–7.11 (t, 6H), 7.17 (s, 2H), 7.22 (s, 1H), 7.3 (s, 3H), 7.36–7.38 (d, 3H), 7.52(s, 3H); ^{13}C NMR ($CDCl_3$, 75 MHz, δ, ppm): 29.40 (s), 29.60 (s), 120.10 (s), 122.81 (s), 123.54 (s), 126.18 (s), 127.20 (s), 130.28 (s), 136.23 (s), 138.23 (s), 145.82 (s), 146.29 (s); MALDI-TOF MS (m/z) Calcd: for $C_{36}H_{30}$, 462.636; found: 462.054.

4.7 Synthesis of Ph-yne-BCB

Add 50 mL of triethylamine and 100 mL of anhydrous tetrahydrofuran into a pre-dried three-neck flask. Add 1,3,5-tribromobenzene (5.127 g, 0.015 mmol) to the solution and dissolve with magnetic stirring. After bubbling with N_2 for 15 min in an ice-water bath to deoxygenate, sequentially add 4-ethynylbenzocyclobutene (8.66 g, 0.0675 mol), $Pd(PPh_3)Cl_2$ (0.63 g, 0.9 mmol), CuI (0.171 g, 0.9 mmol), and PPh_3 (0.472 g, 1.8 mmol), and continue bubbling with N_2 for another 15 min. Under nitrogen protection, slowly raise the temperature of the system to 85 °C and let it react for 12 h. After cooling to room temperature, filter out the insoluble solids from the system, and rotary evaporate to remove excess solvent, yielding a dark brown solid. Dissolve this solid in 100 mL of dichloromethane, extract three times with saturated brine solution, and dry the organic phase with anhydrous magnesium sulfate for 2 h. Filter, rotary evaporate, and perform column chromatography (eluent: dichloromethane/petroleum ether, ratio 1 : 20 to 1 : 5) to obtain a pale yellow product with a yield of 77%.^{1}H NMR ($CDCl_3$, 300 MHz, δ, ppm): 3.20 (s, 12H), 7.03–7.05 (d, 3H), 7.21 (s, 3H), 7.37–7.40 (d, 3H), 7.60 (s, 3H); ^{13}C NMR ($CDCl_3$, 75 MHz, δ, ppm): 29.51 (s), 29.90 (s), 86.96 (s), 91.47 (s), 121.11 (s), 122.67 (s), 124.22 (s), 125.59 (s), 130.76 (s), 133.69 (s), 145.80 (s), 146.74 (s); MALDI-TOF MS (m/z) Calcd: for $C_{36}H_{24}$, 456.588; Found: 456.056.

4.8 Synthesis of TPA-yne-BCB

Add 125 mL of triethylamine and 62.5 mL of anhydrous tetrahydrofuran into a pre-dried three-neck flask. Add tris(4-bromophenyl)amine (3.01 g, 6 mmol) to the solution and dissolve with magnetic stirring. After bubbling with N_2 for 15 min in an ice-water bath to deoxygenate, sequentially add 4-ethynylbenzocyclobutene (3.60 g, 28 mmol), $Pd(PPh_3)Cl_2$ (0.35 g, 0.5 mmol), CuI (47.5 mg, 0.25 mmol), and PPh_3 (98.36 mg, 0.5 mmol), and continue bubbling with N_2 for another 15 min. Under nitrogen protection, slowly raise the temperature of the system to 90 °C and let it react for 12 h. After cooling to room temperature, filter out the insoluble solids from the system, and rotary evaporate to remove excess solvent, yielding a dark brown solid. Dissolve this solid in 100 mL of dichloromethane, extract three times with saturated brine solution, and dry the organic phase with anhydrous magnesium sulfate for 2 h. Filter, rotary evaporate, and perform column chromatography (eluent: dichloromethane/petroleum ether, ratio 1 : 20 to 1 : 5) to obtain a pale yellow product with a yield of 75%. ^{1}H NMR ($CDCl_3$, 300 MHz, δ, ppm): 3.19 (s, 12H), 7.01–7.04 (d, 3H), 7.05–7.07 (d, 6H), 7.20 (s, 3H), 7.36–7.38 (d, 3H), 7.40–7.43 (d, 6H); ^{13}C NMR($CDCl_3$, 75 MHz, δ, ppm): 29.47 (s), 29.85 (s), 88.17 (s), 90.31 (s), 118.21 (s), 121.63 (s), 122.59 (s), 123.99 (s), 124.05 (s), 125.41 (s), 130.55 (s), 132.70 (s), 145.71 (s), 146.17 (s), 146.52 (s); MALDI-TOF MS (m/z) Calcd: for $C_{48}H_{33}N$, 623.799; found: 623.032.

4.9 Synthesis of TPB-yne-BCB

Add 70 mL of triethylamine and 70 mL of anhydrous tetrahydrofuran into a pre-dried three-neck flask. Add 1,3,5-tris(4-bromophenyl)benzene (5.44 g, 0.01 mol) to the solution and dissolve with magnetic stirring. After bubbling with N_2 for 15 min in an ice-water bath to deoxygenate, sequentially add 4- ethynylbenzocyclobutene (6.58 g, 0.05 mol), $Pd(PPh_3)Cl_2$ (0.35 g, 0.5 mmol), CuI (97.2 mg, 0.5 mmol), and PPh_3 (0.26 g, 1 mmol), and continue bubbling with N_2 for another 15 min. Under nitrogen protection, slowly raise the temperature of the system to 95 °C and let it react for 12 h. After cooling to room temperature, filter out the insoluble solids from the system, and rotary evaporate to remove excess solvent, yielding a dark brown solid. Dissolve this solid in 100 mL of dichloromethane, extract three times with saturated brine solution, and dry the organic phase with anhydrous magnesium sulfate for 2 h. Filter, rotary evaporate, and perform column chromatography (eluent: dichloromethane/petroleum ether, ratio 1 : 20 to 1 : 5) to obtain a pale yellow product with a yield of 72%. ^{1}H NMR ($CDCl_3$, 300 MHz, δ, ppm): 3.21 (s, 12H), 7.04–7.06 (d, 3H), 7.25 (s, 3H), 7.41–7.43 (d, 3H), 7.63–7.70 (t, 12H), 7.80 (s, 3H); ^{13}C NMR ($CDCl_3$, 75 MHz, δ, ppm): 29.49 (s), 29.88 (s), 88.20 (s), 91.48 (s), 121.47 (s), 122.64 (s), 122.98 (s), 125.02 (s), 125.54 (s), 127.19 (s), 130.69 (s), 132.07 (s), 140.32 (s), 141.74 (s), 145.76 (s), 146.46 (s); MALDI-TOF MS (m/z) Calcd: for $C_{54}H_{36}$, 684.882; found: 683.956.

4.10 Preparation of the polymer sheets

The mesitylene solution of five target monomers (the overall solid content is 20 wt%) were added to the oven-dried Schlenk tube, respectively. The reaction mixture was heated under the N_2 atmosphere at 160 °C for 24 h after three freeze-pump-thaw cycles. Then the prepolymer solution was allowed to evaporate under vacuum until the solid content is 33 wt%. The concentrated prepolymer was added to the stainless-steel mold (Ø35 mm × 2 mm) for further cross-linking and curing. The mold was permitted to rise to 150 °C in 1 h, 200 °C in 1 h, 260 °C in 1 h and maintained at 260 °C for 3 h. Finally, the cured sheets were cooled to room temperature in a nitrogen atmosphere.

Data availability

The data that supports the findings of this study are available in the ESI† of this article.

Author contributions

Menglu Li – conceptualization, writing – original draft, writing – review & editing. Linfeng Fan – characterization, writing – review & editing. Quan Sun – characterization, writing – review & editing. Meng Xie – characterization, writing – review & editing. Jin Guo – characterization. Wenxin Fu – conceptualization, writing – review & editing, supervision.

Conflicts of interest

The authors declare no conflict of interest.

Acknowledgements

This work was supported by the National Natural Science Foundation of China (No. 52373316, 22075298).

References

1 S. Hong, C. S. Lee, M. H. Lee, Y. Lee, K. Y. Ma, G. Kim, S. I. Yoon, K. Ihm, K. J. Kim, T. J. Shin, S. W. Kim, E. C. Jeon, H. Jeon, J. Y. Kim, H. I. Lee, Z. Lee, A. Antidormi, S. Roche, M. Chhowalla, H. J. Shin and H. S. Shin, Ultralow-dielectric-constant amorphous boron nitride, *Nature*, 2020, **582**, 511–514.

2 M. Li, Q. Sun, W. Fan, X. Lu, J. Sun, Y. Guo, Y. Liu and W. Fu, A bis-stabilized interface strategy for low-k benzocyclobutene-based hollow silica nanocomposites, *ACS Appl. Polym. Mater.*, 2023, **5**, 3698–3706.

3 M. Xie, Y. He, M. Li, W. Fan, Q. Sun and W. Fu, A "bottom-up" strategy for high-performance benzocyclobutene (BCB)-subnanometer inorganic nanocomposites, *ACS Appl. Mater. Interfaces*, 2024, **16**, 54751–54760.

4 W. J. Fan, N. M. Hong, Q. Sun, M. L. Li and W. X. Fu, Thermo-curable and photo-patternable polysiloxanes and polycarbosiloxanes by a facile piers–rubinsztajn polycondensation and post-modification, *Polym. Chem.*, 2022, **13**, 2187–2194.

5 W. J. Fan, M. Xie, J. F. Tian, Y. He, S. Xia and W. X. Fu, Topological design of low dielectric ladder-like polysilsesquioxane and copolymers, *Chin. J. Polym. Sci.*, 2025, **43**, 477–487.

6 Q. Sun, Z. W. Yuan, W. J. Fan, M. L. Li and W. X. Fu, Low dielectric benzocyclobutene-type polymers based on facile synthesis of linear fluorinated monomer, *Chin. J. Polym. Sci.*, 2023, **41**, 1760–1766.

7 D. Zhou, J. Wang, H. Bai, D. Han and Q. Fu, High-performance low-k poly(dicyclopentadiene)-POSS nanocomposites achieved by frontal polymerization, *Chem. Eng. J.*, 2024, **485**, 150140.

8 J. Wang, X. Lin, D. L. Zhou, S. R. Fu, Q. Zhang, H. Bai, D. Han and Q. Fu, High-performance low-k poly(dicyclopentadiene) nanocomposites as achieved via reactive blending with norbornene-functionalized larger POSS, *Macromol. Mater. Eng.*, 2023, **308**, 2300076.

9 E. Milan, G. J. Rees, A. Phillips, C. Cano, Y. Wei, H. Guo, S. Feller and M. Pasta, Lithium antiperovskite-derived glass solid electrolytes, *ACS Mater. Lett.*, 2025, **7**, 1187–1194.

10 H. Zhou, H. Y. Lei, J. H. Wang, S. L. Qi, G. F. Tian and D. Z. Wu, Breaking the mutual restraint between low permittivity and low thermal expansion in polyimide films via a branched crosslink structure, *Polymer*, 2019, **162**, 116–120.

11 G. Song, S. Wang, D. Wang, H. Zhou, C. Chen, X. Zhao and G. Dang, Rigidity enhancement of polyimides containing benzimidazole moieties, *J. Appl. Polym. Sci.*, 2013, **130**, 1653–1658.

12 M. Hasegawa, Y. Watanabe, S. Tsukuda and J. Ishii, Solution-processable colorless polyimides with ultralow coefficients of thermal expansion for optoelectronic applications, *Polym. Int.*, 2016, **65**, 1063–1073.

13 H. Li, P. Wei, Y. Wang, Q. Zhu, X. Wang, W. Gao, L. Tao, K. Ma, Z. Hu and W. Chen, High-frequency 5G substrate: Low dielectric biphenyl polyimide with low CTE and high thermal stability, *Mater. Today Adv.*, 2024, **23**, 100514.

14 Z. Zhou, M. Yu, S. Cao, Y. Huang, Z. Dai, J. Shen, X. Cao, Y. Wang and X. Han, Branched silicone acrylates enhanced photocurable epoxy resins with high strength, toughness, and low dielectric constant for sla 3D printing, *ACS Appl. Polym. Mater.*, 2024, **6**, 2733–2740.

15 H. Lin, X. Lu, A. Lu, M. Yuan and Z. Xin, Preparation of high-performance hyperbranched polybenzoxazine with low dielectric constant, *J. Polym. Sci.*, 2023, **61**, 2333–2343.

16 A. Saadati, M. Hasanzadeh and F. Seidi, Biomedical application of hyperbranched polymers: Recent advances and challenges, *TrAC, Trends Anal. Chem.*, 2021, **142**, 116308.

17 A. B. Cook and S. Perrier, Branched and dendritic polymer architectures: Functional nanomaterials for therapeutic delivery, *Adv. Funct. Mater.*, 2020, **30**, 1901001.

18 G. F. I. Toki, M. K. Hossain, W. U. Rehman, R. Z. A. Manj, L. Wang and J. Yang, Recent progress and challenges in silicon-based anode materials for lithium-ion batteries, *Ind. Chem. Mater.*, 2024, **2**, 226–269.

19 E. Ziemann, J. Qin, T. Coves and R. Bernstein, Effect of branching in zwitterionic polymer brushes grafted from PES UF membrane surfaces via AGET-ATR(c)P, *J. Membr. Sci.*, 2023, **672**, 121422.

20 C. Yoshikawa, R. Takagi, T. Nakaji Hirabayashi, T. Ochi, Y. Kawamura and H. Thissen, Marine antifouling coatings based on durable bottlebrush polymers, *ACS Appl. Mater. Interfaces*, 2022, **14**, 32497–32509.

21 M. Suraj Belgaonkar and B. Kandasubramanian, Hyperbranched polymer-based nanocomposites: Synthesis, progress, and applications, *Eur. Polym. J.*, 2021, **147**, 110301.

22 H. S. Hao, L. Y. Nong, H. F. Yao, Z. Han, Q. S. Li, T. G. Feng and W. D. Zhen, Ultra-low dielectric constant polyimides: Combined efforts of fluorination and micro-branched crosslink structure, *Eur. Polym. J.*, 2021, **143**, 110206.

23 J. W. Lee, S. M. Yoo, D. K. Kim, Y. H. Kim, S. M. Park, N. K. Park, Y. J. So, J. Kim, J. M. Park, M. J. Ko and J. C. Won, Intrinsic low-dielectric constant and low-dielectric loss

aliphatic-aromatic copolyimides: The effect of chemical structure, *Mater. Today Commun.*, 2022, **33**, 104479.

24 W. J. Zhao, X. W. Cao, J. S. Huang, J. W. Wen, Y. He, J. W. Zha, R. K. Y. Li and W. Wu, Construction of micro-branched crosslink fluorinated polyimide with ultra-low dielectric permittivity and enhanced mechanical properties, *eXPRESS Polym. Lett.*, 2022, **16**, 142–151.

25 T. Qin, H. Yang, Q. Li, X. Yu and H. Li, Design of functional binders for high-specific-energy lithium-ion batteries: From molecular structure to electrode properties, *Ind. Chem. Mater.*, 2024, **2**, 191–225.

26 J. He, H. Yang, F. Zheng and S. Yang, Dielectric properties of fluorinated aromatic polyimide films with rigid polymer backbones, *Polymer*, 2022, **14**, 649.

27 J. Li, S. Lv, C. Gong, Y. Zhou and F. Huang, Effect of the linking positions on the benzene ring on properties of poly(silane arylether arylacetylene)s, *J. Polym. Sci.*, 2022, **60**, 3232–3243.

28 G. Huang, J. Sun and Q. Fang, Thermo-crosslinkable molecular glasses towards the low k materials at high frequency, *Mater. Today Chem.*, 2022, **24**, 100782.

29 M. L. Dai, J. Sun and Q. Fang, A fluorinated cross-linked polystyrene with good dielectric properties at high frequency derived from bio-based vanillin, *Polym. Chem.*, 2022, **13**, 4484–4489.

30 H. M. Li, X. M. Wang, Y. Z. Gong, H. B. Zhao, Z. B. Liu, L. Tao, D. Dastan, K. Ma, Z. Z. Hu and M. M. Sun, APDS modified several bisphenol a polyimides with low dielectric constant under high frequency, *J. Polym. Res.*, 2023, **30**, 407.

31 L. Hao, J. J. Chen, T. Ma, J. Cheng, J. Y. Zhang and F. G. Zhao, Low dielectric and high performance of epoxy polymer via grafting POSS dangling chains, *Eur. Polym. J.*, 2022, **173**, 111313.

32 F. P. Liu, J. Sun and Q. Fang, Biobased low-k polymers at high frequency derived from isoeugenol, *ACS Appl. Polym. Mater.*, 2022, **4**, 7173–7181.

33 H. Wang, Z. C. Liu, X. Shang, L. D. Feng, X. C. Bian and X. S. Chen, Crosslinked colorless polyimide films via oxazole groups as crosslinking agent: Preparation and properties, *Chin. J. Polym. Sci.*, 2024, **42**, 1905–1914.

34 L. Shi, F. Bao, Y. Liu, H. Li, T. Zhu, H. Liu, J. Yu, Y. Qiao, C. Zhu and J. Xu, Design and synthesis of low dielectric poly(aryl ether ketone) from incorporation bulky fluorene groups and regular hydroquinone structure, *Langmuir*, 2023, **39**, 11439–11447.

35 A. Sengupta, Y. Koike and Y. Okamoto, Investigation of the physical properties of poly(ortho- and para-trifluoromethoxy styrenes), *Macromol. Chem. Phys.*, 2013, **214**, 1734–1737.

36 X. Sun, G. Mo, L. Z. Zhao, L. H. Dai, Z. H. Wu and M. Q. Jiang, Characterization of nanoscale structural heterogeneity in an amorphous alloy by synchrotron small angle x-ray scattering, *Acta Phys. Sin.*, 2017, **66**, 176109.

37 W. Yu and K. Luo, Polymer translocation through a nanopore driven by binding particles: Influence of chain rigidity, *Phys. Rev. E*, 2014, **90**, 042708.

38 K. Maex, M. R. Baklanov, D. Shamiryan, F. Lacopi, S. H. Brongersma and Z. S. Yanovitskaya, Low dielectric constant materials for microelectronics, *J. Appl. Phys.*, 2003, **93**, 8793–8841.